AD-A169 736 STUDY OF THE PERTURBATION OF THE SURFACE-WAVE HEIGHT SPECTRUM DUE TO A SI..(U) JOHNS HOPKINS UNIV LAUREL MD APPLIED PHYSICS LAB D R THOMPSON JUN 86 1/1

UNCLASSIFIED JHU/APL/TG-1356 N00024-85-C-5301 F/G 8/3 NL

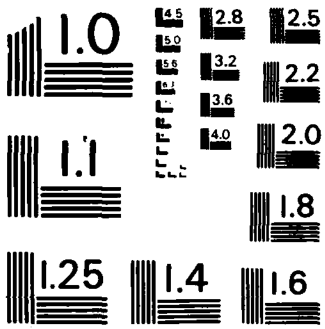

MICROCOPY RESOLUTION TEST CHART
NATIONAL BUREAU OF STANDARDS-1963-A

1

JHU/APL
TG 1356
JUNE 1986

AD-A169 736

Technical Memorandum

STUDY OF THE PERTURBATION OF THE SURFACE-WAVE HEIGHT SPECTRUM DUE TO A SINUSOIDAL CURRENT FEATURE OF VARIABLE WAVELENGTH AND PHASE SPEED

by D. R. THOMPSON

THE JOHNS HOPKINS UNIVERSITY ■ APPLIED PHYSICS LABORATORY

86 7 15 011

UNCLASSIFIED
SECURITY CLASSIFICATION OF THIS PAGE

PLEASE FOLD BACK IF NOT NEEDED FOR BIBLIOGRAPHIC PURPOSES

REPORT DOCUMENTATION PAGE

1a. REPORT SECURITY CLASSIFICATION Unclassified	1b. RESTRICTIVE MARKINGS
2a. SECURITY CLASSIFICATION AUTHORITY	3. DISTRIBUTION/AVAILABILITY OF REPORT Approved for public release; distribution is unlimited.
2b. DECLASSIFICATION/DOWNGRADING SCHEDULE	
4. PERFORMING ORGANIZATION NUMBER(S) JHU/APL TG 1356	5. MONITORING ORGANIZATION REPORT NUMBER(S) JHU/APL TG 1356

6a. NAME OF PERFORMING ORGANIZATION The Johns Hopkins University Applied Physics Laboratory	6b. OFFICE SYMBOL (If Applicable) STS	7a. NAME OF MONITORING ORGANIZATION Naval Plant Representative Office
6c. ADDRESS (City, State, and ZIP Code) Johns Hopkins Road Laurel, Md. 20707		7b. ADDRESS (City, State, and ZIP Code) Johns Hopkins Road Laurel, Md. 20707
8a. NAME OF FUNDING/SPONSORING ORGANIZATION Defense Advanced Research Projects Agency	8b. OFFICE SYMBOL (If Applicable) STO	9. PROCUREMENT INSTRUMENT IDENTIFICATION NUMBER N00024-85-C-5301

8c. ADDRESS (City, State, and ZIP Code)
Arlington, Va. 22209

10. SOURCE OF FUNDING NUMBERS

PROGRAM ELEMENT NO.	PROJECT NO.	TASK NO.	WORK UNIT ACCESSION NO.
		ZDAO	

11. TITLE (Include Security Classification)
Study of the Perturbation of the Surface-Wave Height Spectrum due to a Sinusoidal Current Feature of Variable Wavelength and Phase Speed (U)

12. PERSONAL AUTHOR(S)
Thompson, Donald R.

13a. TYPE OF REPORT	13b. TIME COVERED	14. DATE OF REPORT (Year, Month, Day)	15. PAGE COUNT
Technical Memorandum	FROM ______ TO ______	1986, June	17

16. SUPPLEMENTARY NOTATION

17. COSATI CODES

FIELD	GROUP	SUB-GROUP
08	03	

18. SUBJECT TERMS
wave-current interaction
spectral perturbation
action-balance equation
surface-wave relaxation rate
SAR imaging of internal waves

19. ABSTRACT (Continue on reverse if necessary and identify by block number)

Closed-form expressions for the perturbation of the surface-wave spectrum due to a weak sinusoidal current feature are developed from the general wave-current interaction equations. A parametric study is presented of the dependence of the perturbation on quantities such as the wavelength, phase speed, and propagation direction of the current feature, along with an estimate of the most strongly perturbed spectral component as a function of these parameters. The perturbation due to more complicated features may be obtained from the results presented in this work through Fourier expansion techniques.

20. DISTRIBUTION/AVAILABILITY OF ABSTRACT ☒ UNCLASSIFIED/UNLIMITED ☐ SAME AS RPT. ☐ DTIC USERS	21. ABSTRACT SECURITY CLASSIFICATION Unclassified	
22a. NAME OF RESPONSIBLE INDIVIDUAL Patrick Evans	22b. TELEPHONE (Include Area Code) (301) 953-5403	22c. OFFICE SYMBOL NPRO

DD FORM 1473, 84 MAR

SECURITY CLASSIFICATION OF THIS PAGE
UNCLASSIFIED

JHU/APL
TG 1356
JUNE 1986

Technical Memorandum

STUDY OF THE PERTURBATION OF THE SURFACE-WAVE HEIGHT SPECTRUM DUE TO A SINUSOIDAL CURRENT FEATURE OF VARIABLE WAVELENGTH AND PHASE SPEED

by D. R. THOMPSON

THE JOHNS HOPKINS UNIVERSITY ■ APPLIED PHYSICS LABORATORY
Johns Hopkins Road, Laurel, Maryland 20707

Operating under Contract N00024-85-C-5301 with the Department of the Navy

THE JOHNS HOPKINS UNIVERSITY
APPLIED PHYSICS LABORATORY
LAUREL, MARYLAND

ABSTRACT

Closed-form expressions for the perturbation of the surface-wave spectrum due to a weak sinusoidal current feature are developed from the general wave-current interaction equations. A parametric study is presented of the dependence of the perturbation on quantities such as the wavelength, phase speed, and propagation direction of the current feature, along with an estimate of the most strongly perturbed spectral component as a function of these parameters. The perturbation due to more complicated features may be obtained from the results presented in this work through Fourier expansion techniques.

CONTENTS

List of Illustrations v
Introduction 1
Formulation 1
Discussion 4
Summary and Conclusions 13
References 14

ILLUSTRATIONS

1. k-dependence of the surface-wave relaxation rate, β, and group velocity 5
2. Amplitude factors as a function of k for various internal-wave phase speeds 6
3. Amplitude factor as a function of k for various angles θ between the k direction and the internal-wave propagation direction 7
4. Amplitude factor as a function of k for various angles ϕ between the k direction and wind direction 8
5. Current and corresponding perturbation as a function of position for $k = 30\ m^{-1}$ (middle plot) and $10\ m^{-1}$ (lower plot). The internal-wave phase speed is 0.2 m/sec; the wind speed is 3 m/sec; and the k vector, internal-wave propagation direction, and wind direction are colinear ($\theta = 0°$, $\phi = 0°$) for each case 9
6. Current and corresponding perturbation as a function of position for $k = 30\ m^{-1}$ (middle plot) and $10\ m^{-1}$ (lower plot). The internal-wave phase speed is 0.2 m/sec; the wind speed is 6 m/sec; and the k vector, internal-wave propagation direction, and wind direction are colinear ($\theta = 0°$, $\phi = 0°$) for each case 10
7. Current and corresponding perturbation as a function of position for $k = 30\ m^{-1}$ (middle plot) and $10\ m^{-1}$ (lower plot). The internal-wave phase speed is 0.2 m/sec and the wind speed is 3 m/sec along the k direction ($\phi = 0°$) for each case 11
8. Current and corresponding perturbation as a function of position for a nominal $k = 30\ m^{-1}$ and k optimized for maximum perturbation for $\phi = 0°$ (middle plot) and $\phi = 60°$ (lower plot) 12

INTRODUCTION

The purpose of this study is to examine quantitatively the perturbation in the surface-wave height spectrum due to the interaction of the surface waves with the current field of an internal wave. The problem has been studied elsewhere (e.g., Refs. 1 and 2 and references cited therein), but we feel that there are enough subtleties to warrant further examination. In particular, we want to estimate the component in the surface-wave spectrum that is most strongly perturbed for a given internal-wave phase speed and wavelength.

FORMULATION

We assume that our current field is given by

$$U = -U_0 \sin [k_I (x - C_I t)],\ -\frac{\pi}{k_I} \le x - C_I t \le \frac{\pi}{k_I}$$

$$= 0 \text{ elsewhere.} \tag{1}$$

Equation 1 describes a sinusoidal feature one wavelength ($= 2\pi/k_I$) in extent, propagating along the x axis with phase velocity C_I. This simplified representation of the internal-wave current field contains the features necessary for our purposes and keeps the mathematics relatively uncomplicated. A more realistic internal-wave current field could be given by a linear superposition of terms such as that of Equation 1.

We have shown[3] that the ratio of the perturbed surface-wave height spectrum $S(\mathbf{k};\ \mathbf{x},\ t)$ at position $\mathbf{x}$ and time t in a general two-dimensional current field to the equilibrium spectrum $S_{eq}(\mathbf{k})$ is given by

$$\frac{S(\mathbf{k};\mathbf{x},t)}{S_{eq}(\mathbf{k})} = \frac{1}{1 + P(\mathbf{k};\mathbf{x},t)}, \tag{2}$$

where

$$P(\mathbf{k};\mathbf{x},t) = N_{eq}(\mathbf{k}) \int_{t_0}^{t} k_j' \frac{\partial U_j}{\partial x_i'} \frac{\partial Q_{eq}(\mathbf{k}')}{\partial k_i'} \exp\left[-\int_{t'}^{t} \beta(\mathbf{k}'')\, dt''\right] dt', \tag{3}$$

and $N_{eq}(\mathbf{k})$ is the equilibrium action spectrum. In Eq. 3, the time dependence of $\mathbf{x}$ and $\mathbf{k}$ is determined by the coupled equations,

$$\frac{dx_i}{dt} = \frac{\partial \omega_0}{\partial k_i} + U_i \tag{4a}$$

[1] B. A. Hughes, *Speckle Noise and Pattern Detection in SAR Imagery of Internal Waves*, 81-12, Defense Research Establishment of the Pacific (Dec 1981).

[2] D. R. Thompson and R. F. Gasparovic, "Intensity Modulation in SAR Images of Internal Waves" (to be published in *Nature*, Apr 1986).

[3] D. R. Thompson, "Intensity Modulation in Synthetic Aperture Images of the Ocean Surface and the Wave-Current Interaction Process," *Johns Hopkins APL Tech. Dig.* 6, 346 (1985).

and

$$\frac{dk_i}{dt} = -k_j \frac{\partial U_j}{\partial x_i} , \tag{4b}$$

where U_i is the ith component of the current field and ω_0 is the intrinsic surface-wave frequency given by the gravity-capillary dispersion relation,

$$\omega_0^2 = g|\mathbf{k}| \left[1 + \left(\frac{|\mathbf{k}|}{360} \right)^2 \right] . \tag{5}$$

Also in Eqs. 3 and 4, $Q_{eq}(\mathbf{k}) = 1/N_{eq}(\mathbf{k})$ and repeated indices are summed. The function $\beta(\mathbf{k})$ in Eq. 3 is the so-called relaxation rate, and it depends on wind velocity as well as $\mathbf{k}$. Later, we shall see that the magnitude of the spectral perturbation is quite sensitive to $\beta(\mathbf{k})$.

The equations for the spectral perturbation given above are general, and their solution can be rather complicated. We now want to simplify our particular problem further by assuming that the internal-wave currents are always much less than the group velocity ($= \partial\omega_0/\partial k_i$) of the surface waves. The group velocity for gravity-capillary waves has a minimum value of about 18 cm/sec at a wavelength of around 4 cm. Therefore, if we require U_0 in Eq. 1 to be about 1 cm/sec or less, we can neglect U_i in Eq. 4a. If we further require the current gradient to be small compared to $1/\beta(\mathbf{k})$, we see from Eq. 4b that the percent change in $\mathbf{k}$ over the relaxation time ($= 1/\beta$) will also be small. For 1-m waves, this requires the current gradient ($= k_I U_0$) to be less than around 10^{-3} sec^{-1}. With $U_0 \approx 1$ cm/sec, this requires that $k_I \leq 0.1$ m^{-1} or the wavelength of the internal-wave feature to be greater than about 50 m.

With the internal-wave current given by Eq. 1 and the restrictions on U_0 and k_I discussed above, Eq. 3 reduces to

$$P(\mathbf{k};x,t) = k_I U_0 k_x \frac{\partial \ln N_{eq}}{\partial k_x} \exp(-\beta t) \int_{t_0}^{t} \exp(\beta t') \cos [\, k_I (C_{gx} - C_I) t'] \, dt' , \tag{6}$$

where k_x and C_{gx} denote, respectively, the components of the surface-wave number and group velocity along the x axis. In writing Eq. 6, we have used the relationship $x = C_{gx} t$ obtained by integrating Eq. 4a and neglecting the U_i term. In a coordinate system fixed to the moving current feature, this relationship becomes

$$x = (C_{gx} - C_I)t , \tag{7}$$

where we have assumed that the origin of the two systems coincides at $t = 0$. We may rewrite Eq. 6 in terms of x using Eq. 7 to obtain

$$P(\mathbf{k},x) = \frac{k_I U_0}{C_{gx} - C_I} k_x \frac{\partial \ln N_{eq}}{\partial k_x} \exp\left(- \frac{\beta x}{C_{gx} - C_I} \right)$$

$$\cdot \int_{-\pi/k_I}^{\min(x,\pi/k_I)} \exp\left(\frac{\beta x'}{C_{gx} - C_I} \right) \cos k_I x' \, dx' \tag{8a}$$

for $C_g \geq C_l$ and $x \geq -\pi/k_l$, and

$$P(\mathbf{k},x) = \frac{k_l U_0}{C_{gx} - C_l}\, k_x \frac{\partial \ln N_{eq}}{\partial k_x} \exp\left(-\frac{\beta x}{C_{gx} - C_l}\right)$$

$$\cdot \int_{\pi/k_l}^{\max(x,-\pi/k_l)} \exp\left(\frac{\beta x'}{C_{gx} - C_l}\right) \cos k_l x' \, dx' \tag{8b}$$

for $C_g < C_l$ and $x \leq \pi/k_l$. The integration limits span the region of nonzero current and depend on the sign of $C_g - C_l$, which determines whether x increases or decreases with time. Equations 8 may be integrated to obtain

$$P(\mathbf{k},x) = k_l U_0 \; k_x \frac{\partial \ln N_{eq}}{\partial k_x} \frac{1}{[\beta^2 + k_l^2 \, (C_{gx} - C_l)^2]^{1/2}}$$

$$\cdot \left\{\cos\,(k_l x - \delta) + \cos\delta \exp\left[-\frac{(k_l x + \text{sgn}\,\pi)}{\tan\delta}\right]\right\}, \tag{9a}$$

with

$$\tan\delta = \frac{k_l(C_{gx} - C_l)}{\beta} \tag{9b}$$

and

$$\text{sgn} = \begin{cases} 1 \text{ for } C_{gx} \geq C_l \\ -1 \text{ for } C_{gx} < C_l \end{cases} \tag{9c}$$

for $-\pi/k_l \leq x \leq \pi/k_l$. For $x > \pi/k_i$, we find

$$P(\mathbf{k},x) = -\,(1 + \text{sgn})\, k_l U_0 \; k_x \frac{\partial \ln N_{eq}}{\partial k_x} \frac{\beta}{\beta^2 + k_i^2(C_{gx} - C_l)^2}$$

$$\cdot \sinh\left[\frac{\beta\pi}{k_l(C_{gx} - C_l)}\right] \exp\left(-\frac{\beta x}{C_{gx} - C_l}\right); \tag{9d}$$

for $x < -\pi/k_l$, $P(\mathbf{k},x)$ equals the result in Eq. 9d with the factor $-(1 + \text{sgn})$ replaced by $(1 - \text{sgn})$. Finally, for $x \leq -\pi/k_l$ and $C_g \geq C_l$ or for $x \geq \pi/k_l$ and $C_g < C_l$, $P(\mathbf{k}, x) = 0$.

DISCUSSION

Equations 9 are the desired expressions for the perturbation of the **k**th component of the surface-wave spectrum as a function of position along the current feature. Note that if $C_{gx} = C_I$, these equations reduce to

$$P(\mathbf{k},x) = k_I U_0 \, k_x \, \frac{\partial \ln N_{eq}}{\partial k_x} \, \frac{1}{\beta(\mathbf{k})} \cos k_I x \qquad \text{(10a)}$$

for $|x| \leq \pi/k_I$ and zero otherwise. For a Pierson-Moskowitz height spectrum with a $\cos^n \phi/2$ angular dependence where ϕ is the angle between **k** and the wind direction, we find that

$$k_x \, \frac{\partial \ln N_{eq}}{\partial k_x} = \left[\left(\frac{1.48 g^2}{V_w^4 k^2} - \frac{9}{2} \right) \cos\theta + \frac{n}{2} \tan\frac{\phi}{2} \sin\theta \right] \cos\theta \,, \qquad \text{(10b)}$$

where g is the acceleration of gravity, V_w is the wind speed, and θ is the angle between **k** and the x axis (internal-wave propagation direction). Inserting this expression into Eq. 10a, we obtain

$$P(\mathbf{k},x) = \left[\left(\frac{9}{2} - \frac{1.48 g^2}{V_w^4 k^2} \right) \cos\theta - \frac{n}{2} \tan\frac{\phi}{2} \sin\theta \right] \cos\theta \cdot \frac{1}{\beta(\mathbf{k})} \, \frac{\partial U}{\partial x} \,, \qquad \text{(10c)}$$

where $\partial U/\partial x$ is the current gradient. For wind speeds of about 3 m/sec or more and **k** values corresponding tc waves of 1 m or less propagating in the wind direction ($\phi \approx 0°$), Eq. 10c can be reduced further to

$$P(\mathbf{k},x) = \frac{9}{2} \cos^2\theta \, \frac{1}{\beta(\mathbf{k})} \, \frac{\partial U}{\partial x} \,, \qquad \text{(10d)}$$

an equation that has been used to estimate the modulation observed in Seasat synthetic aperture radar (SAR) images.

From Eqs. 10, we see that the perturbation varies directly as the current gradient and inversely with the relaxation rate $\beta(\mathbf{k})$. However, it is important to remember that Eqs. 10 hold only for the so-called resonance condition when the x component of the group velocity for surface waves of wave number **k** is equal to the phase speed of the internal-wave feature. Thus, for a given **k** value (e.g., determined by the frequency of a radar transmitter), this resonance condition will not, in general, be met, and the expressions given by Eqs. 9 must be used to compute the spectral perturbation. In fact, we will show in the following discussion that the maximum perturbation does *not* usually occur for the **k** value that yields the resonance condition.

In order to understand how the perturbation given by Eqs. 9 varies with **k** for a given current feature, it is useful to first see how $\beta(\mathbf{k})$ and C_g vary with

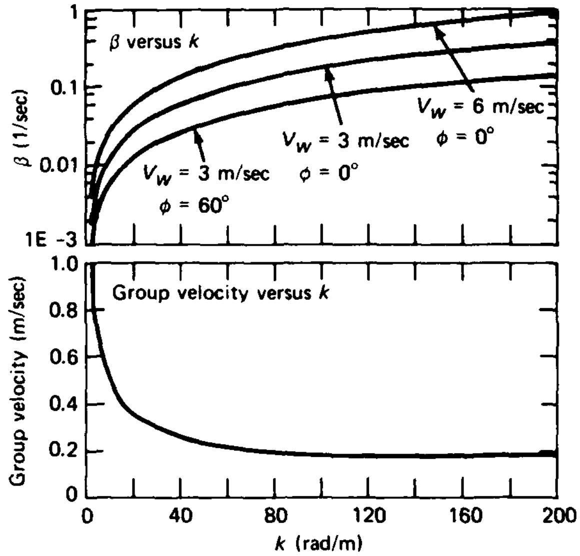

Figure 1 k-dependence of the surface-wave relaxation rate, β, and group velocity. The β curves are for wind speeds V_w of 3 and 6 m/sec and for wind direction with respect to k, $\phi = 0°$ and $\phi = 60°$. The parameterization of $\beta(\mathbf{k})$ is that of Hughes.[4]

k. As discussed in Refs. 3 and 4, the behavior of $\beta(\mathbf{k})$ is a topic of current research. However, we have found recently that the full solution of Eqs. 3 and 4 with $\beta(\mathbf{k})$ given by Hughes[4] yields good agreement with measured spectral perturbation data from the Georgia Strait Experiment.[5] Therefore, we show the **k** dependence of Hughes' $\beta(\mathbf{k})$ in the upper plot of Fig. 1 for wind speeds of 3 and 6 m/sec (measured 10 m above the surface) blowing along the direction of **k** and for 3 m/sec blowing at an angle $\phi = 60°$ from the **k** direction. Note that for all cases shown $\beta(\mathbf{k})$ increases slowly for $k \gtrsim 60$ m^{-1} but decreases rather rapidly for $k \lesssim 60$ m^{-1}. The surface-wave group velocity, shown in the lower plot of Fig. 1, is just the derivative with respect to k of the gravity-capillary dispersion relation given by Eq. 5. It is, in fact, almost constant at about 0.2 m/sec between $k = 60$ and 200 m^{-1} but varies like $k^{-1/2}$ for $k \lesssim 60$ m^{-1} (the gravity-wave region).

Thus we see that for $60 \le k \le 200$ m^{-1}, the entire k dependence in $P(\mathbf{k},x)$ is essentially due to that of $\beta(\mathbf{k})$. Furthermore, for internal-wave wavelengths greater than about 60 m ($k_I \le 0.10$ m^{-1}) and $-0.1 \le C_I \le 0.5$ m/sec, $k_I \cdot (C_g - C_I)$ is small compared to β for roughly $30 \le k \le 200$ m^{-1}. For these conditions, we have essentially the resonance condition, and Eqs. 10 for $P(\mathbf{k},x)$ approximate closely the more general expressions of Eqs. 9.

On the other hand for $k \lesssim 30$ m^{-1}, the **k** dependence of both $\beta(\mathbf{k})$ and C_g must be considered in estimating the maximum perturbation. In Fig. 2, we show

[4]B. A. Hughes, "The Effect of Internal Waves on Surface Wind Waves; Theoretical Analysis," *J. Geophys. Res.* **83C**, 455 (1978).
[5]D. R. Lyzenga and R. A. Schuehman, eds., *Interim Report on the Georgia Strait Experiment*, Vol. I, Environmental Res. Inst. of Michigan (Dec 1984).

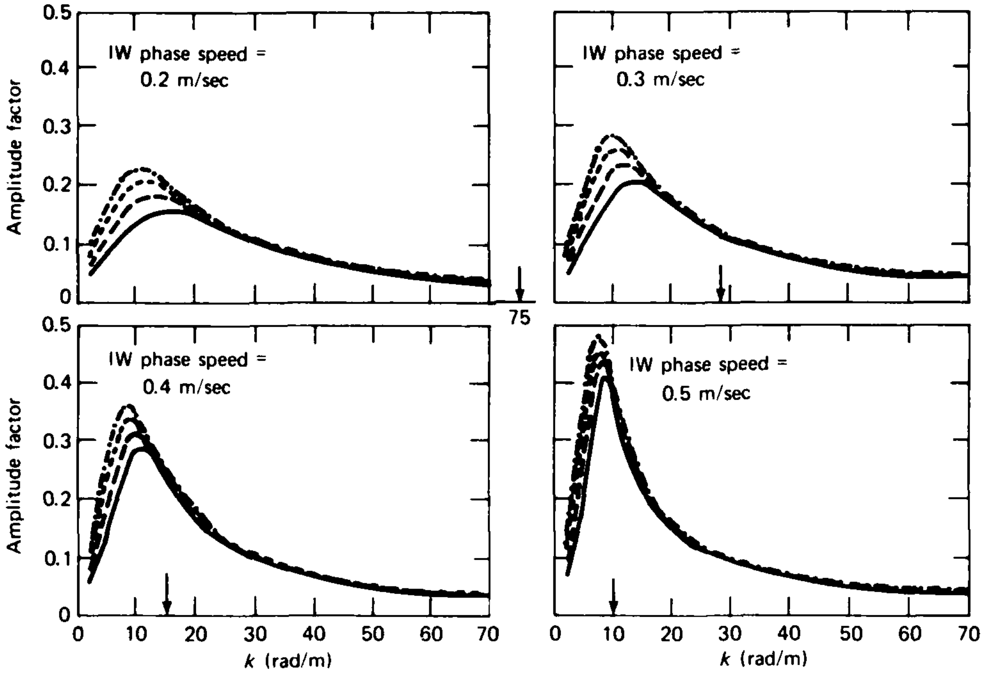

Figure 2 Amplitude factor as a function of k for various internal-wave phase speeds. The four curves (solid, dash, short dash, and dash/dot) in each of the plots are computed for internal-wave wavelengths of 60, 80, 100, and 120 m, respectively. The k vector, internal-wave propagation direction, and wind direction are colinears ($\theta = 0°$, $\phi = 0°$), and the wind speed is 3 m/sec for all cases.

plots of the amplitude factor in Eq. 9a (the term that multiplies the { } brackets) as a function of k for fixed internal-wave phase speeds C_I. The results for various wave numbers k_I corresponding to internal-wave wavelengths of 60, 80, 100, and 120 m are shown by the solid, dash, short dash, and dash/dot curves, respectively. The arrows on the k axis of the plots in Fig. 2 mark the k value for which the resonance condition ($C_{gx} = C_I$) holds. All of the curves in the figure were computed using the $\beta(\mathbf{k})$ corresponding to a 3 m/sec wind along the direction of $\mathbf{k}$ ($\phi = 0°$), and with the angle between $\mathbf{k}$ and the internal-wave propagation direction equal to zero (i.e., $\theta = 0$ and $C_{gx} = C_g$). Also, we have assumed for these and all subsequent computations that the peak current gradient, $k_I U_0 = 10^{-3}$ sec^{-1}, remains constant and that the $k_x \partial \ln N_{eq}/\partial k_x$ term in Eqs. 9 is given by Eq. 10b with $n = 4$.

We can see from Fig. 2 that for $30 \leq k \leq 200$ m^{-1} the amplitude factor is nearly independent of the properties of the internal wave (for the range of k_I and C_I values considered) as expected from our previous discussion, and its variation over this range is due entirely to the behavior of $\beta(\mathbf{k})$. For $k \leq 30$ m^{-1}, we begin to see the dependence of the amplitude factor on k_I and C_I. In particular, we note that for a given C_I, the largest amplitude occurs for the smallest k_I and that the largest amplitudes overall occur for the largest phase speed $C_I = 0.5$ m/sec. This behavior is simply a result of the k dependence of β and C_g in the denominator of the amplitude term in Eq. 9a. Since $\beta(\mathbf{k})$ increases with k faster than C_g decreases, this denominator will always have a minimum at a

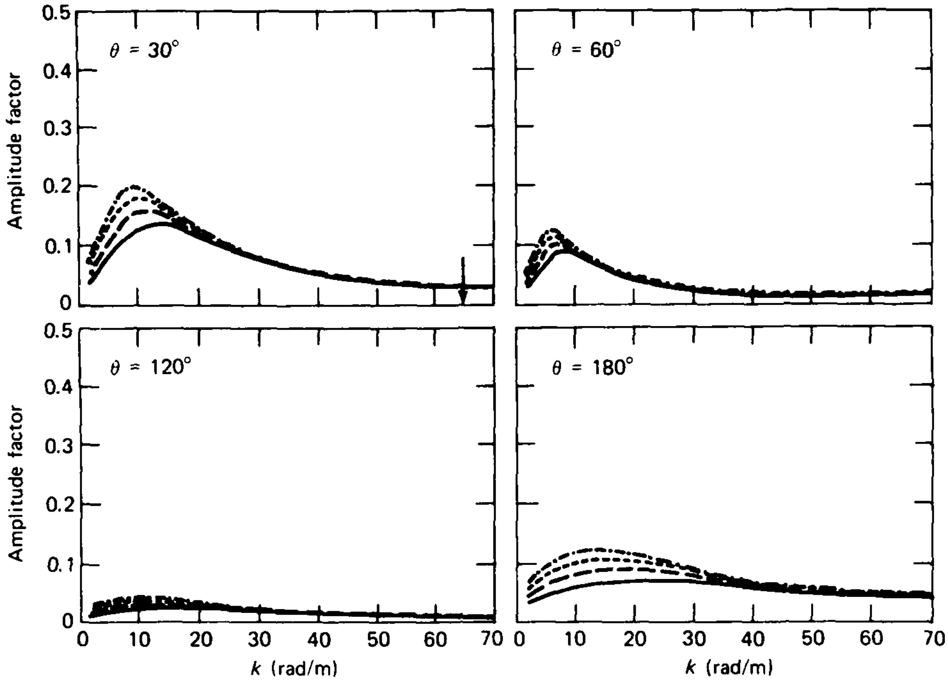

Figure 3 Amplitude factor as a function of k for various angles θ between the k direction and the internal-wave propagation direction. The four curves (solid, dash, short dash, and dash/dot) in each of the plots are computed for internal-wave wavelengths of 60, 80, 100, and 120 m, respectively. The internal-wave phase speed is 0.2 m/sec, and the wind speed is 3 m/sec along the k direction (ϕ = 0°) for all cases.

k value less than that for which $C_g = C_I$. The value of this minimum (which produces a maximum in $P(\mathbf{k},x)$) is, of course, controlled by the value of k_I and C_I for the particular internal wave in question. A decrease in k_I or an increase in C_I will lower the value of this minimum and shift its position to a smaller **k** value.

In Fig. 3, we show how the amplitude factor varies as a function of θ, the angle between **k** and the internal-wave propagation direction. In each of the plots in this figure, we have assumed an internal-wave phase speed of $C_I = 0.2$ m/sec and a $\beta(\mathbf{k})$ corresponding to 3 m/sec winds along the direction of **k** (i.e., $\phi = 0°$), as before. The solid, dash, short dash, and dash/dot curves in each plot are again for internal-wave wavelengths of 60, 80, 100, and 120 m, respectively, and the arrows indicate the **k** value where the resonance condition holds. (There can be no resonance condition for $\theta \geq 90°$.) One can see from the plots in this figure (and the $C_I = 0.2$ m/sec plot in Fig. 2, which is for $\theta = 0°$) that the amplitude factor decreases as θ approaches 90° due to the $\cos^2\theta$ dependence of $k_x \partial \ln N_{eq}/\partial k_x$ (as given by Eq. 10b with $\phi = 0°$). As θ becomes larger than 90°, the $k_I^2\,(C_{gx} - C_I)^2$ term in the denominator of Eq. 9a begins to grow. It can be seen from Fig. 3 that the size of this term along with the $\cos^2\theta$ dependence controls the behavior of the amplitude factor for $\theta \geq 120°$.

Figure 4 illustrates how the wind-direction dependence of $\beta(\mathbf{k})$ can affect the amplitude factor. In each of the plots in this figure, we have again chosen an

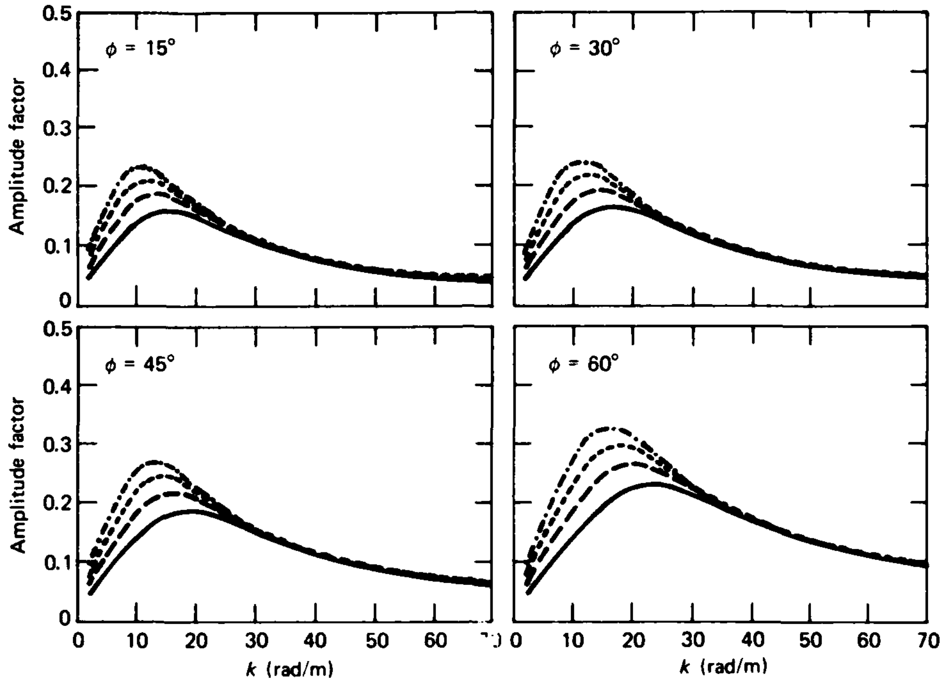

Figure 4 Amplitude factor as a function of k for various angles ϕ between the k direction and wind direction. The four curves (solid, dash, short dash, and dash/dot) in each of the plots are computed for internal-wave wavelengths of 60, 80, 100, and 120 m, respectively. The internal-wave phase speed is 0.2 m/sec, the wind speed is 3 m/sec, and the k direction is along the internal-wave propagation direction (θ = 0°) for all cases.

internal-wave phase speed of C_I = 0.2 m/sec and a wind speed of 3 m/sec as in Fig. 3. For this case, however, we have assumed that the **k** vector is pointing along the x axis (θ = 0°) for each plot and that the wind direction is at an angle ϕ with respect to **k** as indicated. As before, solid, dash, short dash, and dash/dot curves in each plot represent internal-wave wavelengths from 60, 80, 100, and 120 m, respectively. The resonance condition occurs at k = 75 m^{-1}. Since $\beta(\mathbf{k})$ decreases like cos ϕ (see Fig. 1), we see from Fig. 4 that the amplitude factors increase with increasing ϕ as expected. In particular, it can be seen that the **k** value corresponding to the maximum amplitude factor increases with increasing ϕ (decreasing β). For example, as ϕ increases from 0 to 60°, a comparison of the internal-wave wavelength equals 100 m curve in the C_I = 0.2 m/sec plot in Fig. 2 (for which ϕ = 0°) with the corresponding curve in the ϕ = 60° plot in Fig. 4 shows that the position of maximum amplitude moves from 10 to about 18 m^{-1} and increases in magnitude from 0.2 to 0.3.

In order to see how the perturbation varies over the extent of the internal-wave feature, we show in Fig. 5 plots of the assumed internal-wave current (given by Eq. 1) and the resulting spectral perturbation $P(\mathbf{k}, x)$ (given by Eqs. 9) for specified **k** values as a function of x. In constructing the plots shown in Fig. 5, we have chosen an internal-wave wavelength of 100 m, a phase speed of 0.2 m/sec, and a wind speed of 3 m/sec along the propagation direction. The wave number vector of the surface waves is chosen to be 30 and 10 m^{-1} in the mid-

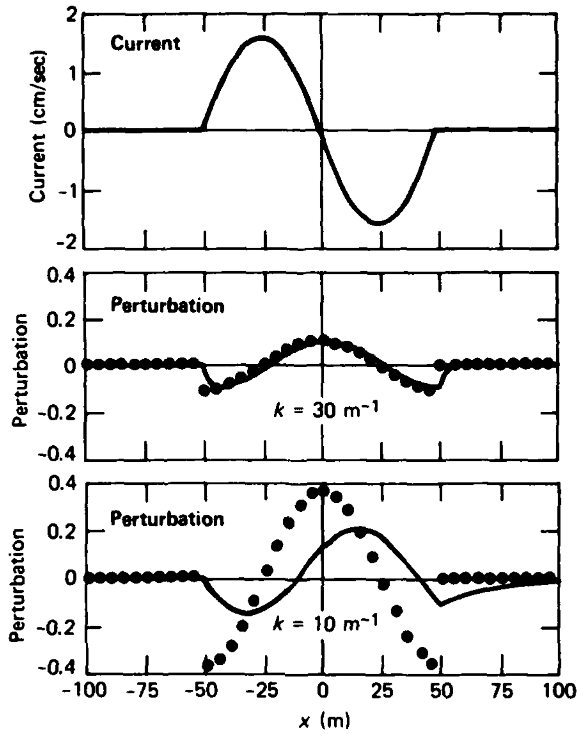

Figure 5 Current and corresponding perturbation as a function of position for $k = 30\ \mathrm{m}^{-1}$ (middle plot) and $10\ \mathrm{m}^{-1}$ (lower plot). The internal-wave phase speed is 0.2 m/sec; the wind speed is 3 m/sec; and the k vector, internal-wave propagation direction, and wind direction are colinear ($\theta = 0°$, $\phi = 0°$) for each case. The • symbol shows the perturbation predicted by the resonance approximation.

dle and lower plots, respectively, with both vectors pointing in the internal-wave propagation direction. (These conditions correspond to $\theta = 0°$ and $\phi = 0°$.) The • symbols in the lower two plots show the perturbations predicted by the resonance approximation given by Eq. 10c. We see from Fig. 5 that, for $k = 30\ \mathrm{m}^{-1}$, the variation of the perturbation as a function of position in the internal-wave current feature given by the resonance condition agrees well with that given by the more general expressions of Eqs. 9. In particular, the perturbation for this case is roughly proportional to the gradient of the current except near the current boundaries where the transient terms in Eqs. 9 are important. On the other hand, for the $k = 10\ \mathrm{m}^{-1}$ case shown in the bottom plot of Fig. 5, we see that the maximum perturbation is increased by about a factor of two over the $k = 30\ \mathrm{m}^{-1}$ case. This increase is smaller by a factor of about two than the increase predicted by the resonance approximation (and shown by the • symbols in the plot), and the position of the maximum perturbation is at $x \approx 15$ m rather than $x = 0$ m due to the phase shift δ that appears in Eqs. 9. Note also that for the $k = 10\ \mathrm{m}^{-1}$ case, there is a non-negligible perturbation extending for about 20 m or so beyond the current boundary at $x = 50$ m, a feature also not predicted by the resonance-condition computations.

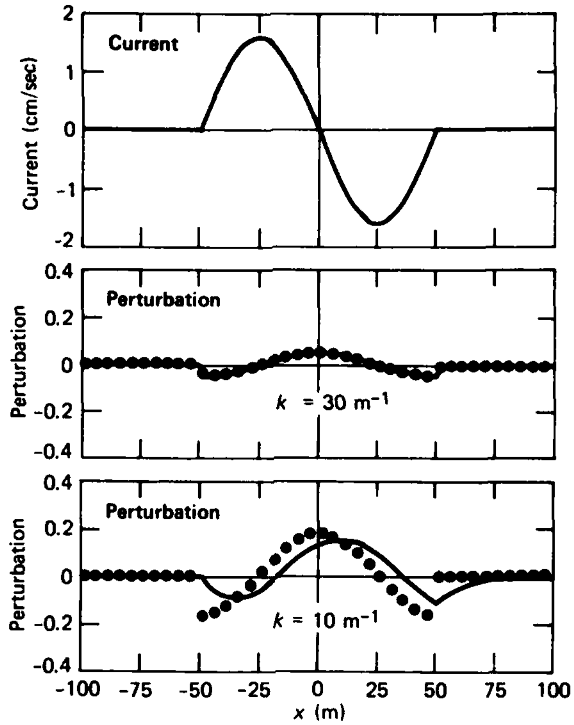

Figure 6 Current and corresponding perturbation as a function of position for $k = 30\ \mathrm{m}^{-1}$ (middle plot) and $10\ \mathrm{m}^{-1}$ (lower plot). The internal-wave phase speed is 0.2 m/sec; the wind speed is 6 m/sec; and the k vector, internal-wave propagation direction, and wind direction are colinear ($\theta = 0°$, $\phi = 0°$) for each case. The • symbol shows the perturbation predicted by the resonance approximation.

Figure 6 was computed in exactly the same manner as Fig. 5 except that a wind speed of 6 m/sec (again in the internal-wave propagation direction) was assumed in the computation of $\beta(\mathbf{k})$. The important feature here is that the resonance approximation gives results that are in closer agreement with the more general computation than were found for the 3 m/sec wind speed. One can see that, for the 6 m/sec wind, the relative increase in the maximum perturbation between $k = 10$ and $30\ \mathrm{m}^{-1}$ is about a factor of three. Also by comparing Figs. 5 and 6, we see that the absolute magnitude of the perturbation (computed using Eqs. 9) decreases by only a factor of about 1.3 in going from 3 to 6 m/sec winds. This is a smaller reduction than the factor of two predicted by the resonance approximation.

We illustrate the difference in $P(\mathbf{k}, x)$ for $\theta = 0°$ and $\theta = 180°$ in Fig. 7, where the middle and lower plots show the comparison for $k = 30\ \mathrm{m}^{-1}$ and $k = 10\ \mathrm{m}^{-1}$, respectively. An internal-wave phase speed of $C_I = 0.2$ m/sec and a wavelength of 100 m were again assumed for these computations, along with a wind speed of 3 m/sec in the $\mathbf{k}$ direction ($\phi = 0°$). The $k = 30\ \mathrm{m}^{-1}$ results are rather similar both in shape and in magnitude. Those for $k = 10\ \mathrm{m}^{-1}$ are

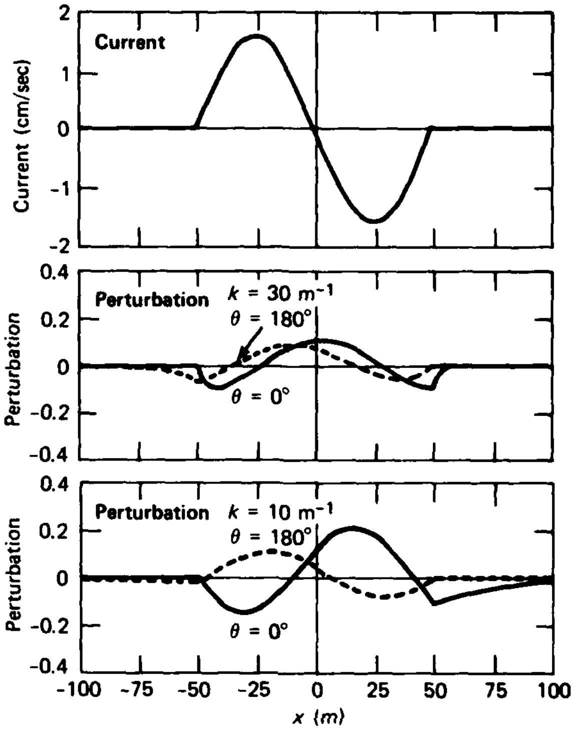

Figure 7 Current and corresponding perturbation as a function of position for $k = 30\ m^{-1}$ (middle plot) and $10\ m^{-1}$ (lower plot). The internal-wave phase speed is 0.2 m/sec and the wind speed is 3 m/sec along the k direction ($\phi = 0°$) for each case. The solid curve in each of the perturbation plots is for k along the internal-wave propagation direction ($\theta = 0°$), while the dashed curve is for k opposite the propagation direction ($\theta = 180°$).

roughly 130° out of phase, with the maximum at $x \approx 15$ m for the $\theta = 0°$ curve being about a factor of two larger than the maximum at $x \approx -20$ m for the $\theta = 180°$ curve. This figure illustrates the fact that the θ dependence of $P(\mathbf{k}, x)$ is more complicated, especially at lower k values, than the simple $\cos^2 \theta$ dependence given by the resonance approximation of Eq. 10c.

As a practical application for the results presented above, we point out that in the context of Bragg scattering theory the intensity modulation observed in the radar image of a particular current feature is expected to be proportional to the perturbation in the surface-wave spectrum at the Bragg wavelength. (For a discussion of Bragg scattering of electromagnetic radiation from a rough surface, see Ref. 6.) For an L-band SAR, for example, the Bragg wavelength is in the 0.2 m range, which corresponds to $k \approx 30\ m^{-1}$. Therefore, if such a radar, looking along the propagation direction, were to image our nominal internal-wave current feature of wavelength 100 m and phase speed 0.2 m/sec, and if

[6] J. W. Wright, "Backscattering from Capillary Waves with Application to Sea Clutter," *IEEE Trans. Antennas Propag.* **AP-14**, 749 (1966).

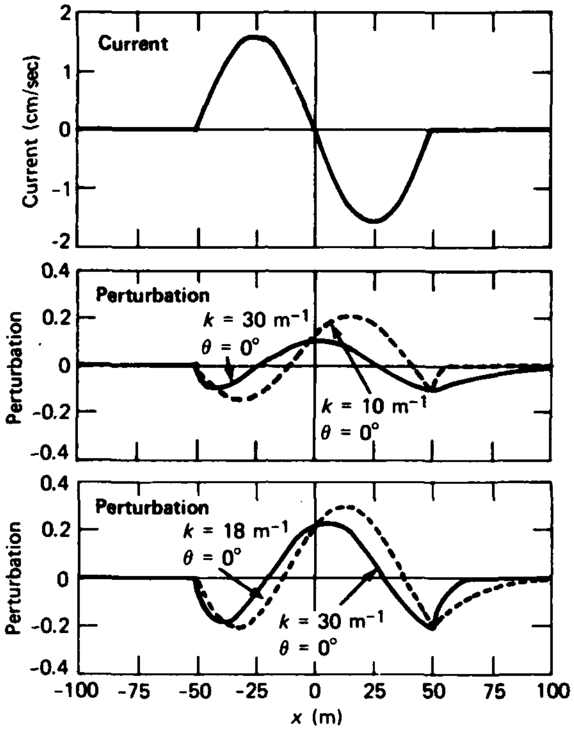

Figure 8 Current and corresponding perturbation as a function of position for a nominal $k = 30\ \text{m}^{-1}$ and k optimized for maximum perturbation for $\phi = 0°$ (middle plot) and $\phi = 60°$ (lower plot). The internal-wave phase speed is 0.2 m/sec, the wind speed is 3 m/sec, and the k direction is along the propagation direction ($\theta = 0°$) for each case.

the wind speed were 3 m/sec also along the propagation direction, we would expect to see an image intensity modulation across the current feature that varies like the solid curve in the middle plot of Fig. 8. However, from our previous discussion we know that the degree of modulation for an internal-wave feature of this type is substantially enhanced at lower k values. In particular, we see from the phase speed = 0.2 m/sec plot in Fig. 2 that the maximum amplitude factor for a 100 m feature occurs at about $k = 10\ \text{m}^{-1}$. Thus, by "tuning" our radar to a wavelength of about 0.63 m (which corresponds to $k = 10\ \text{m}^{-1}$), we would expect to see the intensity modulation given by the dashed curve in the middle plot of Fig. 8. By tuning to this "optimum frequency," we obtain a factor of two gain in the maximum perturbation and also increased modulation (brighter, since $P(\mathbf{k}, x) < 0$) for $x > 50$ m outside the current feature as shown in this plot.

The bottom plot in Fig. 8 shows a similar example for which the wind is assumed to be blowing at 60° to the propagation direction and radar look direction (i.e., $\theta = 0°$ and $\phi = 60°$). The solid curve in this plot shows the expected intensity modulation for $k = 30\ \text{m}^{-1}$, while the dashed curve shows the modulation for the optimum $k = 18\ \text{m}^{-1}$ obtained from the $\phi = 60°$ plot in Fig. 4. One can see that the $k = 30\ \text{m}^{-1}$ modulation is already larger than the cor-

responding $\phi = 0°$ case due to the decrease in $\beta(\mathbf{k})$ with increasing ϕ. However, an additional factor of 1.5 can be gained in the maximum modulation by tuning to $k = 18\ m^{-1}$. Also, as was seen for the $\phi = 0°$ case, this tuning yields a substantial increased brightening outside the current feature for $x > 50$ m.

We conclude that for given wind conditions, internal-wave properties, and viewing geometry, one can, at least in principle, tune a radar as illustrated in the above examples to obtain the optimum intensity modulation in the image. Conversely, it may also be possible to use a knowledge of the return signal (along with viewing geometry and wind conditions) to deduce the properties of the current feature.

SUMMARY AND CONCLUSIONS

In this study, we have developed closed-form expressions for the perturbation of a two-dimensional surface-wave height spectrum due to a one-dimensional sinusoidal current feature with specified wavelength and phase speed. These expressions were derived from a general formulation of the wave-current interaction problem,[3] with the restriction that only currents whose magnitude is less than a few centimeters per second and whose gradient magnitude is less than a few $10^{-3}\ sec^{-1}$ be considered. The expressions have been checked against the general calculation for a number of different cases (which satisfy the above restrictions), and excellent agreement was found in each case.

We have used these expressions to examine how the magnitude of the spectral perturbation depends on quantities such as the surface-wave wave number and propagation direction, internal-wave phase speed and wavelength, and wind speed and direction. The study showed that regimes exist where the perturbation is sensitive to changes in each of these parameters. We have also found that the so-called resonance approximation for the spectral perturbation, which is exact when the surface-wave group velocity is equal to the phase velocity of the current feature, is reasonably valid for surface-wave numbers greater than about 30 m^{-1} with wind speeds greater than about 3 m/sec. However, as the magnitude of the wave number decreases below 30 m^{-1}, the resonance approximation breaks down rather quickly, and the more general expressions must be used to obtain accurate estimates of the perturbation.

The behavior of the perturbation as a function of position across the current feature has also been examined as a function of the various parameters, and it was found that the position of the maximum and minimum values, for example, can be quite sensitive to changes in these parameters. In particular, we have seen that, for the combination of parameters that yield the largest magnitude perturbation, the position of the maximum (or minimum) is usually not at the position of maximum (or minimum) current gradient. This is in contrast to the resonance approximation that predicts that the perturbation should vary like the current gradient. Furthermore, it was found that, in many cases, significant perturbation can exist well beyond the extent of the current feature—again in contradiction to the resonance approximation.

Finally, we have shown how it may be possible, at least in the context of Bragg scattering theory, to tune the frequency of a radar using our results in order to maximize the observed intensity modulation from a given current feature. On

the other hand, it may also be possible to invert our equations using the observed radar return at several different frequencies to determine the properties of the current feature. Although we feel that the results presented in this study are quite reliable for signal characterization, it is clear that a more complete knowledge of the statistics of the radar return from a no-current background region is required before more quantitative conclusions can be made. However, with continued effort, our understanding of the complex problems involved in the remote sensing of surface current features should expand quite rapidly.

REFERENCES

[1] B. A. Hughes, *Speckle Noise and Pattern Detection in SAR Imagery of Internal Waves,* 81-12, Defense Research Establishment of the Pacific (Dec 1981).

[2] D. R. Thompson and R. F. Gasparovic, "Intensity Modulation in SAR Images of Internal Waves" (to be published in *Nature*, Apr 1986).

[3] D. R. Thompson, "Intensity Modulation in Synthetic Aperture Images of the Ocean Surface and the Wave-Current Interaction Process," *Johns Hopkins APL Tech. Dig.* **6**, 346 (1985).

[4] B. A. Hughes, "The Effect of Internal Waves on Surface Wind Waves; Theoretical Analysis," *J. Geophys. Res.* **83C**, 455 (1978).

[5] D. R. Lyzenga and R. A. Schuehman, eds., *Interim Report on the Georgia Strait Experiment,* Vol. I, Environmental Res. Inst. of Michigan (Dec 1984).

[6] J. W. Wright, "Backscattering from Capillary Waves with Application to Sea Clutter," *IEEE Trans. Antennas Propag.* **AP-14**, 749 (1966).

INITIAL DISTRIBUTION EXTERNAL TO THE APPLIED PHYSICS LABORATORY

The work reported in TG 1356 was done under Navy Contract N00024-85-C-5301. This work is related to Task ZDAO, which is supported by Defense Advanced Research Projects Agency (STO).

ORGANIZATION	LOCATION	ATTENTION	No. of Copies
DEPARTMENT OF DEFENSE			
DTIC/FDRB	Alexandria, VA		12
DEPARTMENT OF THE NAVY			
NAVSEASYSCOM	Washington, DC	SEA-9961	2
NAVAIRSYSCOM	Washington, DC	AIR-7226	2
NAVPRO	Laurel, MD		1
U.S. GOVERNMENT AGENCIES			
DARPA	Arlington, VA	D. Lewis (STO)	1

Requests for copies of this report from DoD activities should be directed to DTIC/FDRB, Cameron Station, Bldg. 5, Alexandria, Virginia 22304-6145 using DTIC Form 1 and, if necessary, DTIC Form 55.

*Initial distribution of this document within the Applied Physics Laboratory has been made in accordance with a list on file in the APL Technical Publications Group.

END

DTIC

8-86